

Research Article

Open Access

Marco Bernardi, Can Ataca, Maurizia Palumbo, and Jeffrey C. Grossman*

Optical and Electronic Properties of Two-Dimensional Layered Materials

DOI 10.1515/nanoph-2015-0030

Received May 9, 2015; accepted December 1, 2015

1 Introduction

Modern semiconductor devices have revolutionized wide-ranging technologies such as electronics, lighting, solar energy, and communication [1]. The semiconductor industry employs Si to fabricate electronic circuits, and GaAs, GaN, and other III–V materials for optoelectronics [2], with typical substrates consisting of wafers manufactured at high temperature. Precisely controlled thin films can be deposited on the substrate to achieve additional functionality, for example by chemical vapor deposition (CVD) or molecular beam epitaxy [3].

Recent research has focused on a new generation of atomically thin films of semiconducting materials. Guided by the rise of graphene [4–7] – itself a semimetal – a broad family of two-dimensional (2D) semiconducting materials have been fabricated in monolayer, bilayer, and few-layer form [8, 9]. Monolayer 2D materials can be prepared by exfoliating layered crystals in which the layers are held together by weak van der Waals forces [5], or in select cases by CVD [10–12]. While exfoliation is still the main choice in scientific research, CVD fabrication will be important to scale up manufacturing of 2D materials to large areas.

***Corresponding Author: Jeffrey C. Grossman:** Department of Materials Science, Massachusetts Institute of Technology, 77 Massachusetts Avenue, Cambridge, MA 02139, USA, E-mail: jcg@mit.edu

Marco Bernardi: Department of Applied Physics and Materials Science, Steele Laboratory, California Institute of Technology, Pasadena, CA 91125, USA, E-mail: bmarco@caltech.edu

Can Ataca: Department of Materials Science, Massachusetts Institute of Technology, 77 Massachusetts Avenue, Cambridge, MA 02139, USA

Maurizia Palumbo: Department of Materials Science, Massachusetts Institute of Technology, 77 Massachusetts Avenue, Cambridge, MA 02139, USA

and ETSF, Department of Physics, University of Rome Tor Vergata, Via della Ricerca Scientifica 1, 00133 Rome, Italy; INFN, Laboratori Nazionali di Frascati, Via E. Fermi 40, 00044 Frascati, Italy

Monolayer and few-layer semiconductors possess novel combinations of optical and electronic properties [7, 8, 13, 14], and thus present a unique opportunity in condensed matter research and semiconductor devices. New physics arises in 2D semiconductors, largely due to the peculiar electronic structure and screening in 2D systems. As the techniques to grow 2D materials on large areas continue advancing, the new properties of these materials may enable a paradigm shift in semiconductor-based technologies, and lead to flexible and ultrathin electronic [14, 15] and optoelectronic devices [16].

This review covers the state of the art in the optical and electronic properties of 2D materials, with a focus on semiconducting systems. Metallic monolayers are also discussed briefly. Our aim is to highlight a few essential concepts emerging from the vast and rapidly growing literature on 2D materials, and suggest future research directions and challenges.

2 Electronic Structure

The optical properties of materials are largely determined by their electronic band structure and screening [17–19], which are the subjects of the next two sections. We begin with a brief review of graphene since much of the emphasis on 2D materials has originated from work on this system. Graphene is a 2D crystal of carbon atoms arranged in a hexagonal honeycomb lattice. The electronic structure of graphene is easily derived from a tight binding model, resulting in peculiar Dirac cones at the corners of the Brillouin zone [7]. Near these points, the electron dispersion is described by a linear relation $E = \pm v_F p$, where E and p are the electron energy and momentum, $v_F = 10^6$ m/s is the Fermi velocity, and the plus and minus signs refer to the conduction and valence bands, respectively. The bands with conical dispersion intersect at the Fermi energy, thus making graphene a semimetal. The conical dispersion of low-energy carriers in graphene is very different from the usual parabolic dispersion in bulk semiconductors, and can be mapped to an effective 2D Hamiltonian for massless Dirac fermions [7]. Bilayer graphene is also a

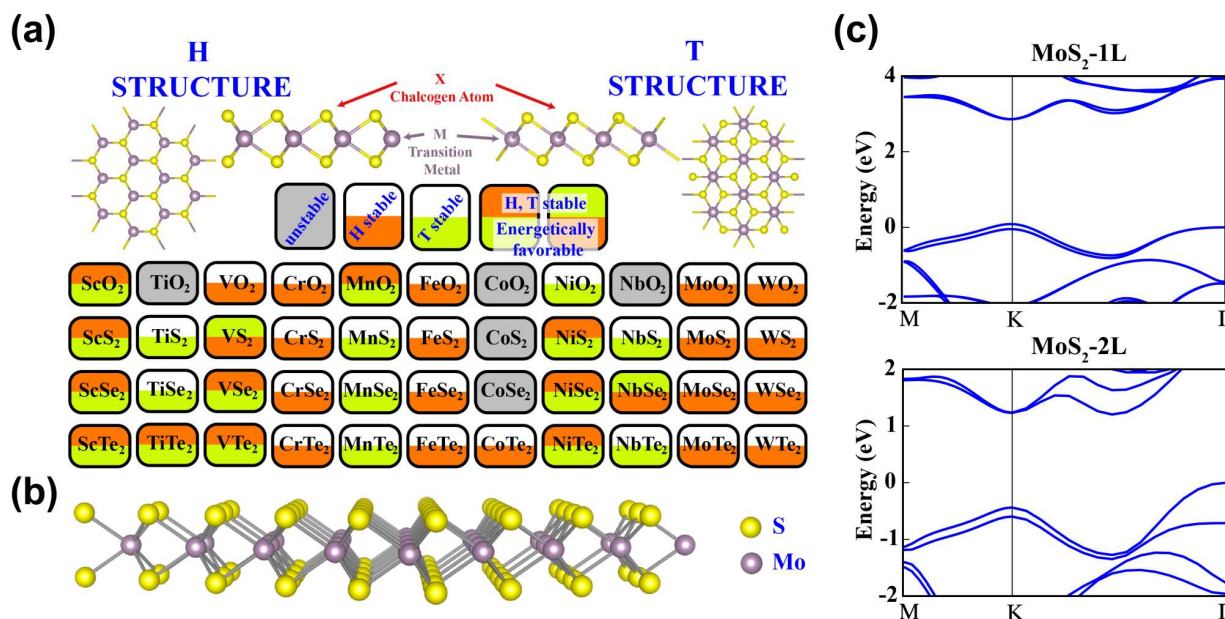


Figure 1: TMD monolayers with formula MX_2 , where M is a transition metal of group 4–10 and X is a chalcogen (or oxygen). The monolayers are classified according to their stability in the H or T structures, where H is the most common structure with D_{3h} symmetry and trigonal prismatic metal coordination, and T indicates a structure with D_{3d} symmetry and octahedral metal coordination (see Ref. 26). Unstable structures are shown in gray. **(b)** The structure of monolayer MoS_2 , shared by the other group-6 TMDs. **(c)** Band structure of monolayer and bilayer MoS_2 , computed using DFT plus GW. The band structures of MoSe_2 , WS_2 , and WSe_2 are qualitatively similar to the ones of MoS_2 shown here.

semimetal, though with parabolic dispersion at the Fermi energy and a small band gap of up to 250 meV that can be opened with an electric field [20, 21]. Extensive work has been carried out to predict theoretically and search experimentally novel physical effects stemming from the peculiar band structure of graphene. This work was recognized in the 2010 Nobel Prize in Physics to Andre Geim and Konstantin Novoselov [22], and opened a new exciting chapter in materials science, chemistry, and condensed matter physics research. Excellent reviews exist on the vast literature related to monolayer and bilayer graphene [7].

Intrinsic graphene does not have free carriers since valence and conduction bands touch at the Fermi level, yet chemical doping and electrostatic gating can both generate electron or hole carriers. Several limitations to the technological applicability of graphene remain, largely due to the absence of a band gap in this material [23, 24]. Digital electronics, field effect transistors, and optoelectronics at visible frequencies are examples of technologies where materials with a band gap are highly preferable, and for which graphene in its pure form may fall short as a novel ultrathin material [23, 24]. On the other hand, graphene may excel in other applications such as fast analog electronics and radio-frequency transistors [23, 24].

Following the pioneering work on graphene, a host of metallic, semiconducting, and insulating monolayers have been prepared by exfoliation and CVD [8–13]. Studies of micron-scale flakes complemented by theoretical calculations have highlighted a range of novel electronic and optical properties in these materials. Recent research has focused on a family of metallic and semiconducting materials with chemical formula MX_2 , where M is a transition metal of group 4–10 and X is a chalcogen such as S, Se, or Te [25]. These materials are known as transition metal dichalcogenides (TMDs).

Out of approximately 40 2D-TMDs that have been studied experimentally or predicted to be stable theoretically [26], some are metallic (e.g., VS_2 and NbS_2) and others are semiconducting (e.g., MoS_2 and WS_2) or insulating (e.g., HfS_2) [25, 26] (see Figure 1a). Semiconducting TMDs have received significant attention due to their tunable band gap and optical properties. In particular, group-6 monolayer TMDs are direct gap semiconductors, while their bilayers and thicker multilayers exhibit an indirect gap. For example, MoS_2 [8, 13, 27], MoSe_2 [28], WS_2 , and WSe_2 [29] all undergo a crossover from indirect to direct gap when going from bilayer to monolayer (see Figure 1c).

The atomic and electronic structure of group-6 TMD monolayers has been studied extensively [8, 26, 27]. Mono-

layer MX_2 consists of a layer of M atoms sandwiched between two atomic layers of X atoms, with a hexagonal unit cell with D_{3h} symmetry and a thickness of ~ 0.7 nm [25, 26] (see Figure 1b). The bilayers and multilayers can have different vertical stacking [25, 26], the most energetically favorable of which is the AB stacking (also known as 2H stacking) commonly found in bulk MoS_2 crystals. The atomic structure of 2D-TMDs has been reviewed recently [25].

The band gaps of group-6 monolayer TMDs are in the 1–2 eV range, ideal for optoelectronic applications. The band gap increases for increasing size of the chalcogen atom, and is less sensitive to the size of the transition metal. For example, typical values of the optical band gaps are 1.9 eV (MoS_2), 1.65 eV (MoSe_2), 2 eV (WS_2), and 1.7 eV (WSe_2) [8, 13, 28–30]. The valence band maximum (VBM) and conduction band minimum (CBM) are located at the K point corner of the hexagonal Brillouin zone (BZ) and are mostly contributed by the d orbitals of the transition metal atom [25]. Spin–orbit coupling splits the VBM into two states with a well-defined spin projection, S_z , in the out-of-plane direction [31, 32], an effect more evident in W-based than in Mo-based TMDs due to the higher mass of W.

Due to lack of inversion symmetry in monolayer TMDs, there are two inequivalent K points in the BZ, called here K_{\pm} . Time-reversal symmetry requires the VBM to be degenerate at K_{\pm} and the value of S_z at K_+ to be opposite to the value at K_- . The band structure of bilayer group-6 TMDs shows the formation of an indirect gap due to the interaction of antibonding p_z orbitals from X atoms in the two TMD monolayers, resulting in an increase of the VBM energy at Γ [8]. The VBM and CBM at K show contributions only from localized d orbitals of the transition metal [8, 25]. Simple crystal field models of a transition metal atom with trigonal prismatic coordination to chalcogen atoms can capture the qualitative trends and character of the band edge electronic states in 2D-TMDs [25], similar to the case of transition metal oxides [33].

Band structure calculations of 2D-TMD materials have been carried out in several works using density functional theory (DFT) [34]. When semilocal approximations of electronic exchange and correlation are employed, then for the specific case of 2D-TMDs, DFT can capture the main trends of the band structure [8, 26], though the electronic band gap is underestimated and the band dispersions need slight corrections [27, 35] to match photoemission experiments. More accurate band structure calculations carried out with the GW method (where G is the Green's function, and W the screened Coulomb potential) [19] show large corrections up to 0.5–1 eV to the DFT band gap. DFT

with properly tuned nonlocal (hybrid) exchange correlation functionals such as HSE-06, B3LYP, and PBE0 have also been employed to improve the accuracy of DFT band gap calculations [36].

The band gap computed with GW is a quasiparticle gap [18, 19], and as such agrees closely with the electronic gap measured in scanning tunneling spectroscopy and photoemission experiments. The gap measured in optical absorption experiments can be modeled by taking into account the electron–hole interaction using the Bethe–Salpeter equation (BSE) [18]. For the case of monolayer MoS_2 , DFT with the local density approximation (LDA) yields a gap of ~ 1.6 eV [8], a GW gap of ~ 2.8 eV [27, 35], and a BSE gap of ~ 1.9 eV [35, 37] in agreement with the experimental absorption onset in MoS_2 . Taken together, the GW-BSE method can correctly predict the quasiparticle and absorption gaps with ~ 0.1 – 0.2 eV accuracy, and it has become the tool of choice for accurate calculations of optical and electronic properties in 2D materials. The difference between the GW quasiparticle and BSE absorption gap is a good approximation of the binding energy of the lowest-energy exciton. Using this approach, the binding energy of excitons in group-6 2D-TMDs has been estimated in several works (see below).

The effect of temperature, doping, and defects on the band structure of 2D-TMDs are very important for electronic and optoelectronic applications, as discussed next. Since in bilayer and thicker group-6 TMDs the indirect (Γ to Γ -K) and direct (K to K) gaps have similar values (Figure 1c), temperature variations can change the optical and electronic properties of TMDs [38]. For example, in few-layer MoSe_2 where the indirect and direct gaps are nearly degenerate, a temperature rise can effectively drive the system toward a 2D regime by thermally decoupling neighboring layers via interlayer thermal expansion [38]. Increasing the interlayer spacing reduces the coupling between the layers and leads to an increase in the indirect gap, while the direct gap at K is not affected as it stems from d states localized on the transition metal. Using this approach, Tongay et al. [38] have shown an increase in light emission in few-layer MoSe_2 of a similar magnitude as that seen when going from bilayer to monolayer MoS_2 [8]. The change in the in-plane and interlayer lattice parameters can be accurately predicted using DFT, and probed experimentally with Raman measurements [38].

Adsorption of chemical species can also tune the electronic and optical properties of TMDs [39]. Multiple adsorption sites are available in monolayer TMDs due to the presence of three atomic layers, leading to observation of adatoms adsorbed both on surface sites and at interstitials close to the transition metal atoms (see Figure 2a).

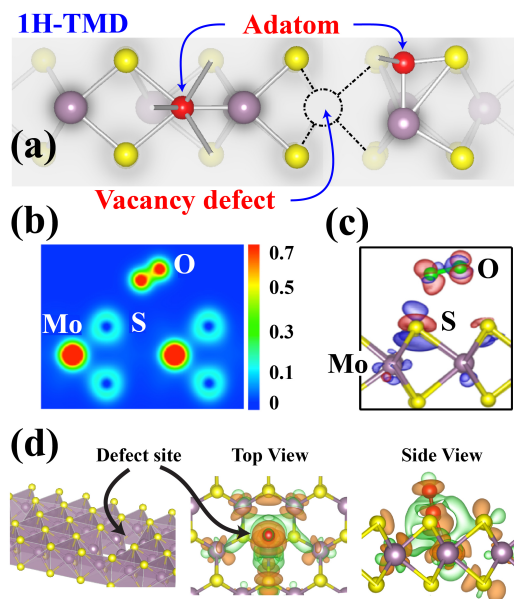


Figure 2: (a) Defect sites in monolayer TMDs, shown for an adsorbed adatom and a vacancy. Purple, yellow, and red spheres are the transition metal, chalcogen, and adatom, respectively. (b) Charge density distribution of an O_2 molecule physisorbed on the surface of MoS_2 . The color scale is in units of $e/\text{\AA}^3$. (c) Charge density difference between pristine MoS_2 and MoS_2 with O_2 physisorbed on its surface. Red indicates charge accumulation and blue charge depletion. (d) Monolayer MoS_2 with a S_2 vacancy, together with top and side views of charge density difference plots of monolayer MoS_2 with a S_2 vacancy interacting with a N_2 molecule (red). Orange denotes charge accumulation and green charge depletion.

At low concentrations, adatoms give rise to localized electronic states in the band gap or resonant states within the bands. Depending on the energy and character of the dopant states, a range of effects can be induced by the impurities including additional optical transitions involving defect states, trapping of carriers and excitons, and enhancement or suppression of scattering channels leading to order of magnitude changes in carrier mobility (see below).

Reactions with oxygen and water to alter the optical properties of TMDs have been studied extensively (see below). DFT calculations showed that the binding energy of physisorbed O_2 or H_2O molecules is ~ 100 meV, and that a charge of 0.04 electrons per O_2 and 0.01 electrons per H_2O is transferred to the molecules, thus depleting monolayer MoS_2 [39] (see Figure 2b, 2c). The transferred charge can increase significantly if the adsorption occurred at a defect site such as sulfur vacancy. A large barrier of ~ 2 eV exists to transition from physisorption to chemisorption, so that physisorption is thought to be the primary adsorption mechanism for O_2 and H_2O . The electron depletion from adsorption of electronegative molecules such as O_2 and

H_2O can lead to dramatic changes in the electrical and optical properties [39]. Adsorption of other chemical species has also been investigated. For example, a joint experimental and computational study [40] showed that N_2 adsorbed on MoS_2 leads to different effects depending on the adsorption site and the presence of S_2 divacancies. While adsorption of N_2 on pristine monolayer MoS_2 adds defect states that are too deep (~ 10 eV) below the Fermi energy to affect the optical and electronic properties, adsorption on S_2 divacancies leads to the appearance of two levels ~ 0.2 eV away from the band edges, which are thought to be responsible for changes in the optical properties of MoS_2 in a N_2 -rich environment [40] (see Figure 2d). Taken together, these results point to the existence of a strong interplay between defects and chemical dopants in 2D-TMDs, which may extend to other 2D materials.

Stacking two or more different monolayers leads to novel possibilities to control the electronic structure. Hetero-bilayers composed of two vertically stacked TMD monolayers of different types are of key importance in optoelectronics and electronics, and have been investigated extensively both for fundamental studies and applications. Hetero-bilayers are analogous to heterojunction interfaces in conventional semiconductors [41], with the difference that in 2D systems the thickness of a bilayer is of order 1 nm and thus lower than the Debye screening length. For this reason, tunneling across a bilayer is possible due to the small thickness, and the substrate critically influences the electronic properties of hetero-bilayers. Similar to bulk semiconductor heterojunctions, the VBM and CBM of the composing semiconductors can achieve either type-I or type-II (staggered) alignments [41] at the interface (see Figure 3), leading to a range of electrical and optical responses. In particular, a type-II alignment leads to the VBM being located on one monolayer, and the CBM on the other monolayer composing the hetero-bilayer material [37]. This particular band alignment is ideal for applications where charge transfer from one layer to the other is important, including lasers and solar cells among others.

The DFT band structures of group-6 hetero-bilayers of MoX_2/WX_2 (with $X = S, Se$) show the presence of an indirect gap due to the interaction between the antibonding p_z orbitals of the composing TMD monolayers, similar to the case of a bilayer of a single TMD material. The VBM at K shows contributions only from d orbitals of WX_2 , and the CBM at K only from d orbitals of MoX_2 , consistent with the formation of a type-II band alignment [37, 42, 43]. The inclusion of band structure corrections with the GW method increases the gap of the individual monolayers by ~ 0.5 – 1 eV but does not change the type-II alignment predicted

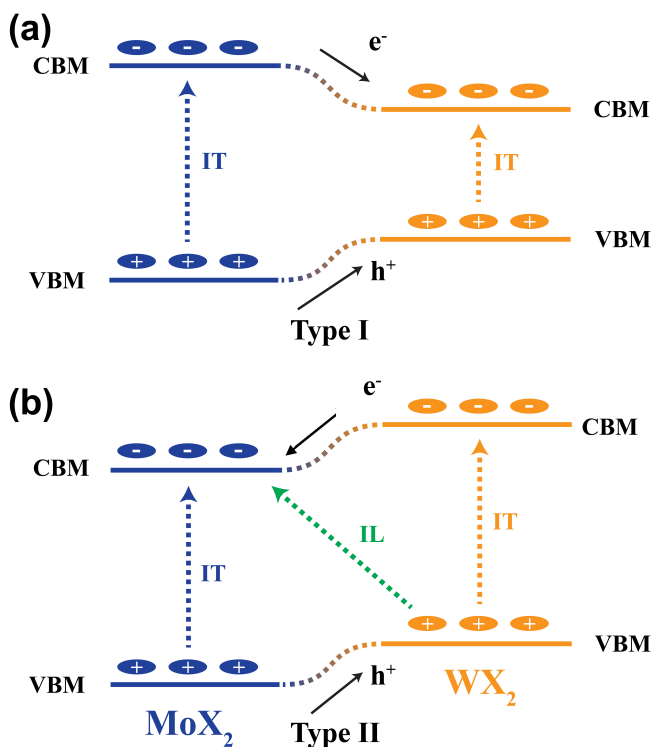


Figure 3: Type-I (a) and type-II (b) band alignments at hetero-bilayer interfaces. Shown are the VBM and CBM energy levels of each monolayer composing the interface, together with the direction of the electron (e^-) and hole (h^+) transfer at the interface. IT and IL indicate, respectively, intralayer and interlayer optical transitions.

within DFT [44], similar to what was found in previous studies of 2D material interfaces [45].

The formation of type-II alignment in MoX_2/WX_2 hetero-bilayers and the resulting charge transfer / separation have been predicted with GW-BSE calculations by our group [37] and others [42, 43], and recently observed experimentally [46]. The type-II alignment found in TMD hetero-bilayers implies that absorption of a photon in either of the composing monolayers can lead to separation of the photogenerated electron and hole, provided the exciton does not recombine before dissociating at the interface. For example, light absorption in WX_2 results in rapid injection of an electron into MoX_2 , while absorption in MoX_2 leads to injection of a hole into WX_2 (see Figure 3). As discussed below, interesting optical effects arise due to the type-II alignment in TMD hetero-bilayers, including ultrafast exciton dissociation and the formation of interlayer excitons with energy lower than the absorption onset of the isolated layers.

Charge separation and rectifying junctions are also possible in hetero-interfaces composed by a 2D metal – such as graphene – and a 2D semiconductor by the for-

mation of a Schottky barrier. For example, using DFT with the band lineup method, we predicted the formation of a Schottky barrier in the MoS_2 –graphene interface [37]. Our calculations show the formation of a Schottky barrier of 1.2 eV for holes to diffuse from graphene to MoS_2 , thus implying that charge separation at the MoS_2 –graphene interface is possible by injecting photogenerated electrons from the conduction band of MoS_2 to graphene, while holes photogenerated in the valence band of MoS_2 are prevented to diffuse to graphene due to the large Schottky barrier [37]. This electron injection mechanism from MoS_2 to graphene upon illumination has been confirmed experimentally [47].

The findings summarized here seem to suggest that in several 2D systems the band alignment type (i.e., type-I or type-II) can be predicted in qualitative agreement with experiment using DFT. Quantitative calculations of band offsets are significantly more complex. GW corrections to the band gap of the single materials plus band alignment using DFT interface dipoles appears to be a viable route for large systems [44, 45, 48]. Studies in which entire interfaces are computed using GW are still challenging due to computational cost. While a bilayer with a unit cell of a few atoms can be computed within GW [27], GW studies of bilayers with twisted or misaligned vertical stacking and multilayer systems are computationally very demanding. We believe that further work is necessary on accurate computations of band offsets in 2D hetero-interfaces.

3 Dielectric Screening

Similar to 0D and 1D nanomaterials, electronic screening in 2D materials is dramatically different than in bulk materials. In the basic picture of screening, a test charge placed in the material polarizes the surrounding medium by applying forces on the electrons and nuclei [49]. In a bulk metallic system, the additional charge is completely screened within a Thomas–Fermi length of a few Angstroms, and the macroscopic field vanishes within the metal. In the case of a bulk semiconductor or insulator, a test charge Q is partially screened by a polarization charge, $-Q(1 - 1/\epsilon)$, where ϵ is the static dielectric constant [49]. However, in 2D materials these simple models break down since the field lines from the test charge extend outside the material into the vacuum, where no screening is possible. Therefore a 2D metal may not screen a test charge completely, while in 2D semiconductors screening is reduced by the presence of vacuum.

Detailed microscopic models of the dielectric function $\epsilon(\mathbf{q}, \omega)$ dependent on wavevector \mathbf{q} and frequency ω reveal complicated trends. At small \mathbf{q} in the in-plane direction, calculations predict that the screening function $\epsilon^{-1}(\mathbf{q})$ shows a marked dip [50], a feature that can be explained using simple models of screening for a 2D sheet in a 3D environment. As a consequence, GW and optical property calculations employing screening converge more slowly than experience with 3D systems would suggest, and sufficient sampling of the Brillouin zone requires very fine grids [50]. Unconverged grids will fail to sample the screening dip and result in overscreening errors. We believe this feature is at least partly responsible for the different values reported in the literature for the GW gaps and exciton binding energies of 2D-TMDs.

As a result of reduced screening, peculiar optical properties arise in 2D materials. Electron–hole pairs generated by optical absorption interact strongly due to the reduced screening, leading to bound electron–hole pairs (excitons) with large binding energy of over 0.5 eV in TMD monolayers [35, 37, 51, 52]. Such strongly bound excitons need not be localized as in the case of Frenkel excitons in molecular systems [49], and can possess radii of over 1 nm, as seen in MoS₂ and MoSe₂ [35, 52]. Surface plasmon (SP) resonances are also strongly affected by the reduced dimensionality [53–55]. For example, the electric field in a SP of a 2D material will decay into vacuum in the layer-normal direction rather than in a dielectric medium [53], thus leading to differences in the electromagnetic energy confinement. As the thickness of a continuum metal slab is reduced, SPs from the two surfaces can couple and form new modes. Peculiar SP dispersions can therefore be expected in 2D materials [54, 55].

Lastly, most experiments are performed on 2D materials supported by substrates, and thus additional screening from the substrate is present. A simple model introduces the effect of the substrate as an additional static screening. For a 2D material between two substrates having dielectric constants of ϵ_1 and ϵ_2 , the substrate screening can effectively be modeled by a single material with a dielectric constant of $\epsilon = (\epsilon_1 + \epsilon_2)/2$. For the case of a material supported by a substrate with dielectric screening ϵ_S , the resulting screening will thus be induced by a dielectric constant of $(\epsilon_S + 1)/2$. More accurate models that take into account the frequency and wavevector dependence of the screening from the substrate appear to improve agreement with experiment for the exciton binding energy of a substrate supported monolayer [52].

4 Light Absorption and Excitons

Light absorption in 2D materials can be surprisingly more intense than in bulk crystals [37]. It can be quantified by the absorbance, namely the fraction of light absorbed at a given frequency. The absorbance can be measured on suspended flakes using transmission or differential reflectance measurements [13, 56], and computed using the GW-BSE approach with an appropriate postprocessing of the dielectric function data [37, 57]. Although a single layer of graphene appears to be visually transparent, it is actually an excellent visible light absorber, achieving 2.3% visible light absorbance in just 3 Å thickness [56], a figure roughly equivalent to the absorbance of a 5–10 nm thick GaAs film [37]. TMD monolayers are also extraordinary light absorbers. The three TMD monolayers MoS₂, MoSe₂, and WS₂ can absorb up to 5–10% incident light at visible frequencies in a thickness of less than 1 nm [13, 37, 58], thus achieving one order of magnitude higher visible light absorption than GaAs.

The high optical absorption at visible energies in TMD monolayers can be explained by dipole transitions with large joint density of states and oscillator strength between localized *d* states with strong spatial overlap on the transition metal atoms [37, 58]. Such transitions are dipole-allowed in a regime of weak spin–orbit coupling, as exhibited by group-6 TMDs. The independent-particle picture explaining absorption in terms of vertical transitions [58] is only partially complete, since excitonic effects in TMD monolayers give rise to a strong mixing of electron–hole configurations in the excited-state wavefunction, leading to a constructive superposition of the oscillator strengths for transitions near the absorption onset [37]. Due to the very high optical absorption in the visible frequency range, 2D-TMDs are among the best sunlight absorbers [37], and applications in photovoltaics and photocatalysis have been recently envisioned for these materials (see below).

The optical response in 2D monolayer semiconductors is dominated by excitonic effects [35, 37, 51, 52]. Due to the reduced dimensionality and weak dielectric screening, excitons can be observed in experiments at room temperature, and possess binding energies more than one order of magnitude higher than those in bulk semiconductors. This implies that the electronic (i.e., quasiparticle) gap is significantly larger than the band gap observed in optical absorption experiments. In the case of group-6 2D-TMDs, large exciton binding energies of 0.5–0.8 eV have been predicted with the GW-BSE method and measured experimentally [35, 37, 51, 52]. These values are similar to those found

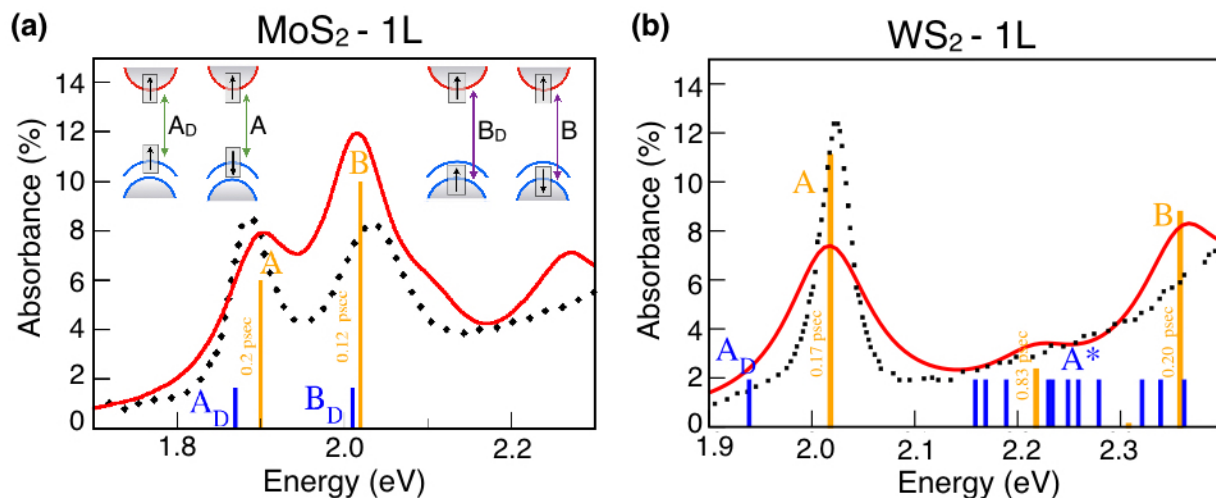


Figure 4: Optical absorption in monolayer MoS₂ (a) and monolayer WS₂ (b). Shown are the experimental (black dots) and computed (red lines) absorbance spectra. The bright A and B excitons are shown in yellow, together with their intrinsic 0 K radiative lifetimes obtained from the BSE (see Ref. [62]). The A_D and B_D dark excitons and the A* dark excitons in WS₂ are shown in blue. The inset in (a) shows the dipole-allowed and dipole-forbidden transitions at a given set of valleys (say, K₊). The transitions at K₋ (not shown) are the time-reversal of those shown here. The data are taken from Ref. [62].

in carbon nanotubes, organic molecules, and some quantum dots, a trend due in all cases to the weak dielectric screening. Even though they are strongly bound, the excitons in 2D-TMDs are of the Wannier type and thus delocalized over several unit cells. For example, the radius of the lowest-energy exciton in MoS₂ and MoSe₂ have been computed to be of order ~ 1.5 nm [35, 52]. Excitons in 2D materials can be bright or dark in character, depending on whether they can be excited or not by light absorption in the linear regime, respectively, as dictated by the dipole selection rules [17]. Dark excitons can be accessed, among other techniques, using two-photon absorption, which has different selection rules than one-photon absorption.

The absorbance spectra of group-6 2D-TMDs monolayers are characterized by the presence of two low-energy excitonic peaks (called A and B, in order of increasing energy) that arise from vertical transitions at the K point of the BZ, from the spin-orbit-split valence band to an almost doubly degenerate conduction band [13, 59] (see Figure 4). The energy of the bright A exciton corresponds to the onset of optical absorption. Heavier chalcogen atoms induce a red shift of the A and B peaks both in MoX₂ and WX₂ TMDs (X = S, Se). Replacing Mo with W while keeping the same chalcogen atom has a relatively small influence on the A exciton, while the energy difference of the B and A peaks increases from 150 meV for MoX₂ to 450 meV for WX₂ (Figure 4) as a consequence of the larger spin-orbit interaction in W-based compared to Mo-based monolayers [31].

The low-energy bright excitons A and B are nearly azimuthally symmetric and resemble the 1s state in a 2D hy-

drogenic model [35], and are each accompanied by a dark exciton at slightly lower energy (Figure 4). A very intense absorption peak, known as the C peak, is present around 2.5–3 eV in all the group-6 TMD monolayers. The C peak is associated with a band nesting in the Γ -K direction [13, 60], and marks the onset of the continuum regime in which excitonic states are closely spaced in energy, have almost zero binding energy, and are associated with uncorrelated electron-hole pairs (i.e., free carriers). In the W-based TMD monolayers, BSE calculations show the presence of a rich series of mostly dark excitons at energies between the A and B peaks (A* excitons in Figure 4), made up by holes from the VBM and electrons from the CBM and the band above the CBM [61, 62]. This series of dark excitons has been recently probed using two-photon absorption and photoluminescence in monolayer WS₂ [61].

At low temperature, an additional absorption peak, identified as a negatively charged exciton, i.e., a three-particle excitation also known as a “trion”, has been observed a few tens of meV below the A exciton in MoS₂, MoSe₂, and WSe₂ monolayers [39, 40, 63, 64]. The trion binding energies in 2D-TMDs are significantly larger than those measured in quantum wells of conventional semiconductors, as a result of the strong Coulomb interaction and weak dielectric screening in 2D materials [63].

Doping, strain, temperature, and the substrate can all affect the optical spectrum of 2D-TMDs. Modulation of the optical properties of 2D-TMDs by doping [40, 65] and strain [66, 67] have been shown in recent work. Temperature-dependent absorption measurements

revealed that the energies of the trion and A and B excitons red-shift by several tens of meV as the temperature is increased from 5 K to 363 K. BSE calculations explained this behavior as the result of thermal expansion of the in-plane lattice constant [68]. While the presence of a substrate [61] red-shifts the absorption peaks only slightly in the monolayers, a sizeable reduction of the electronic band gap and exciton binding energy due to the substrate has been predicted using GW-BSE calculations and confirmed by recent experiments [52, 61]. The optical properties of two or more vertically stacked 2D-TMD monolayers have been studied extensively. In spite of the direct-to-indirect gap crossover, the absorption spectra of bilayer and bulk TMDs present features similar to the corresponding monolayer materials, including the presence of the A and B peaks, which are just slightly altered by the combined effect of interlayer and spin-orbit interactions [69]. The reason for this peculiar behavior is that the states at K giving rise to the lowest-energy excitons are only marginally affected by interlayer interactions. The effect of layer stacking on the energy of the A and B peaks is a slight red shift upon increasing the number of layers due to an increasing exciton delocalization in the layer-normal direction [60, 62].

The resulting absorbance in bilayer and few-layer 2D-TMDs is approximately the sum of the absorbances of the individual composing layers [13, 37], similar to the case of graphene [56]. While this trend has been verified in most 2D-TMDs for a thickness up to three to four layers [13], it is unclear whether the linear increase in absorbance holds for thicker multilayers up to the bulk. For example, we have recently estimated that in graphene the linear trend cannot be extrapolated to the absorption of graphite [37].

Absorption in hetero-bilayers formed by stacking different types of monolayers can differ from the simple sum described above. In particular, optical transitions are found at lower energy than the absorption onset in the individual monolayers composing the mixed bilayer (Figure 3b) [37, 62, 70]. This feature is a signature of interlayer (IL) excitons associated with a hole localized on one layer and an electron on the other layer composing the bilayer material. IL excitons are typically a consequence of type-II interface band alignment, and have been recently observed in optical spectra of hetero-bilayers both experimentally [71, 72] and in GW-BSE calculations [37, 62, 73]. For the case of MoS_2/WS_2 and $\text{MoSe}_2/\text{WSe}_2$, BSE calculations have shown that the lowest-energy IL exciton is composed of a hole localized on the W-based and an electron localized on the Mo-based monolayer [37, 62, 73], and that two bright IL excitons are present due to spin-orbit coupling [62]. The IL excitons found in 2D-TMDs are analogous to the so-called charge-transfer excitons

in donor-acceptor interfaces employed in organic photovoltaics [74], as well as to the indirect excitons observed over a decade ago in quantum wells of GaAs/AlGaAs and other III-V semiconductors [75]. As discussed below, IL excitons are characterized by long lifetimes owing to the spatial separation of the electron and hole, and are thus interesting in applications such as photovoltaics and photocatalysis in which dissociating excitons before recombination is of crucial importance.

We close this section by briefly discussing three topics related to light absorption in 2D-TMDs. First, the absence of inversion symmetry combined with the spin-orbit interaction in group-6 TMD monolayers leads to a locking of the valley and spin quantum numbers. Monolayer TMDs possess two different sets of valleys, called above K_{\pm} , each associated with a specific spin quantum number [32]. Selective excitation of one valley can be achieved with circularly polarized light as a consequence of optical selection rules [76–79], and leads to excitation of carriers with well-defined spin and valley quantum numbers. This so-called valley polarization regime is relevant in valleytronics technologies aiming to employ carriers with a well-defined valley quantum number [77–79]. The idea is analogous to electronics and spintronics – in which a given type of charge or spin orientations are employed – with the difference that carriers in a specific valley would only participate in transport. Experiments of valley polarization using circularly polarized light in group-6 monolayer TMDs have been shown by several groups [77–79] and constitute an active area of investigation in 2D semiconductors.

Second, 2D semiconducting and metallic materials show strong, broadband photocurrent responses [58, 80]. In 2D-TMDs, this effect is a consequence of the strong optical absorption [37] and large joint density of states from the d orbitals [58]. In graphene, the origin of the photoreponse has been studied extensively using graphene junctions [80, 81] and more recently in biased but otherwise homogeneous graphene [82]. Photocurrent in graphene junctions has been attributed to either thermoelectric or photovoltaic effects, while the intrinsic photoreponse in graphene has been attributed to both photovoltaic and bolometric effects, depending on the operating conditions [82]. Due to a bottleneck for electron-phonon scattering – resulting from the low density of states near the Fermi energy – transport of long-lived hot carriers plays an important role in photocurrent experiments in graphene [81–84], and the mechanism for hot carrier cooling is still somewhat controversial [82, 84].

Lastly, the coupling of light to surface plasmons in 2D systems is an active research area. Although the plasmonic excitation in graphene was demonstrated only re-

cently [54, 85, 86], there are already many reports on novel designs of graphene plasmonics for optical applications [54, 85, 86]. Surface plasmons in metallic and doped semiconducting 2D-TMDs are being actively investigated both experimentally and theoretically [87]. Semiconducting 2D materials with different valence and conduction band dispersions are expected to show different surface plasmon dispersions for n and p doping, a feature absent in graphene due to the electron–hole symmetry [88].

5 Light Emission

Light emission in 2D-TMDs changes significantly with number of layers and stacking sequence. While the electronic structure and optical absorption are well understood in 2D-TMDs, much less is known about radiative recombination and exciton dynamics, which are the subjects of the next two sections. As explained above, group-6 2D-TMDs undergo a crossover from indirect to direct gap when going from bilayer to monolayer. As a result, monolayer 2D-TMDs are significantly brighter than bilayers, multilayers, and bulk [8, 13, 30]. Despite the higher brightness of TMD monolayers, the quantum yield of suspended monolayer TMDs prepared by exfoliation is still relatively low. For example, the quantum yield of suspended monolayer MoS₂ has been shown to be of order 0.1% [13], with higher figures shown recently for WS₂. Competing nonradiative processes quenching light emission are likely due to the presence of native defects (e.g., S vacancies) and impurities in exfoliated flakes.

Enhancement of PL in monolayer TMDs can be obtained with a variety of strategies. Recent work has shown that a simple ambient annealing treatment at 200–400°C can enhance light emission in monolayer MoS₂ by up to two orders of magnitude [89]. The proposed mechanism behind PL enhancement is the formation of Mo–O bonds upon ambient annealing. Such substitutional O defects in MoS₂ are thought to induce p doping and localize excitons, thus resulting in more efficient radiative recombination [89]. PL enhancement can also be induced by exposing monolayer MoS₂ to O₂ and H₂O gases [40], consistent with the conjectured role of Mo–O bonds in enhancing PL. Gating [64] and chemical doping [65] have also been shown to enhance PL by providing additional carriers for radiative recombination, but this enhancement is lower than that achieved by annealing or exposure to O₂. Introduction of chalcogen vacancies also increases PL, although this effect disappears when the experiment is performed in vacuum [39]. Most proposed mechanisms for PL

enhancement invoke the equilibrium between trions, excitons, and free carriers as a function of doping to explain changes in PL. More work needs to be done to ascertain the microscopic mechanisms regulating PL in 2D-TMDs. Taken together, these recent findings suggest that light emission in 2D-TMDs can be tuned extensively by defect engineering. An interesting corollary is that, contrary to conventional wisdom, the optical quality of 2D-TMDs may not be a valid criterion to assess crystal quality as in the case of conventional bulk semiconductors [39].

Other strategies investigated to tune PL in 2D-TMDs propose to alter the local electric field at the monolayer rather than the intrinsic radiative and nonradiative rates regulating the quantum yield. The local field enhancement is typically achieved by exciting surface plasmons in metallic nanostructures fabricated in the proximity of the monolayer. Experiments in this area are often complemented by numerical solution of Maxwell's equations to estimate the enhancement of the local electric field. Ref. [90] reviews recent efforts in this area.

Intense research efforts exist to enhance PL in 2D-TMDs with all the strategies mentioned above. The ultimate goal would be to achieve a controllable and inexpensive route to make TMD monolayers significantly brighter than those exfoliated from bulk crystals. Bright, atomically thin TMDs could find application in novel light emission devices, displays, and photonic and optoelectronic technologies. The recent award of the 2014 Nobel Prize in Physics [91] for the utilization of the bulk semiconductor GaN as a blue emitter highlights the relevance of the physics behind light emission, and encourages studies of a novel generation of 2D light emitters.

6 Ultrafast Carrier and Exciton Dynamics

Significant work has been carried out to characterize excited state dynamics in 2D materials using transient absorption and PL techniques [46, 71, 77–79], and more recently first principles calculations [62]. We briefly review recent work on group-6 2D-TMDs. Time-resolved experiments found a range of characteristic times for exciton dynamics in monolayer TMDs. Transient PL experiments suggest that radiative exciton recombination in monolayer TMDs occurs at ultrafast time scale of 1–10 ps at low temperature (4 K) [92, 93] and slower time scale of 0.1–1 ns at room temperature [94, 95]. At room temperature, multiple decay times have been observed [94], and the shortest times of order ~5 ps have been attributed to exciton trap-

ping at defects. We recently carried out first principles calculations on ideal, defect-free 2D-TMDs by extending the GW-BSE method to compute exciton radiative lifetimes. Our calculations show agreement within 5–10% with the measured PL times, and provide rich microscopic information to interpret the experimental time constants [62].

Radiative recombination in bulk and bilayer is slower than in monolayer 2D-TMDs. For example, experiments [94] and calculations [62] found that radiative recombination is approximately two to three times slower in bilayer and bulk than in monolayer MoS₂, a trend attributed to the delocalization of the A exciton in the layer-normal direction leading to lower dipole matrix elements and thus higher radiative lifetimes [62]. Competing non-radiative processes present in the bilayer and bulk due to the indirect gap justify the much lower quantum yield in these systems than in monolayers [8, 13].

Recent work on MoX₂/WX₂ (X = S, Se) hetero-bilayers has shown the presence of very long-lived (~1.5 ns at 20 K [62, 71] and ~30 ns at room temperature [62]) IL excitons constituted by electrons localized on the Mo-based and holes on the W-based monolayer. Our calculations predicted long-lived IL excitons in these hetero-bilayers with lifetimes in excellent agreement with experiments [62]. As a consequence of the type-II band alignment, excitation of either monolayer constituting the MoX₂/WX₂ hetero-bilayer has been shown to result in charge transfer with ultrafast times of ~50 fs [46]. Similar time scales have been previously observed for charge transfer in donor-acceptor type-II interfaces between organic molecules [74, 96–98], suggesting that similar physical processes occur at type-II organic and 2D monolayer interfaces. In both these kinds of interfaces, the time scale for charge transfer competes with exciton thermalization. In donor-acceptor blends of organic molecules with type-II band alignment, charge transfer has been shown to occur from hot excitons with energy higher than the absorption onset, with an important role from IL (i.e., charge transfer) excitons acting as a gateway in the process [74, 96–98]. These findings have contributed to resolve the problem of how carriers bound in excitonic states with over 0.5 eV binding energy, as typical in organic molecules, can break free of the Coulomb interaction and be injected across the interface. Since the binding energy of the excitons decreases dramatically with increasing energy above the absorption onset, the hot excitons involved in the charge transfer may have significantly lower binding energy, and the presence of the charge transfer excitons may also favor the charge transfer. Similar questions regarding the observation of charge transfer in spite of the large exciton binding energy are arising in

the 2D-TMD community, and we believe that much can be learned about the problem from studies of charge transfer in donor-acceptor junctions of organic molecules [74, 96–98].

In closing, we note that the attribution of the observed signals to radiative and nonradiative processes can be ambiguous in time-resolved spectroscopies since defects and impurities can modulate the excited state dynamics. In TMDs, the interpretation of time signals and comparison among different experiments is further complicated by the use of μm size flakes in which the edges can play a significant role in exciton recombination. First principles calculations combining DFT and the GW-BSE method are ideally suited to study excited state dynamics in layered 2D-TMDs. These approaches can accurately predict excited state properties in the energy domain such as band gaps, exciton energies, and absorption/loss spectra, and there is significant promise to extend these methods to study excited state processes in the time domain [99–102].

The studies of ultrafast dynamics in 2D-TMDs discussed here demonstrate that the radiative lifetimes can be tuned over several orders of magnitude with number of layers, stacking sequence, and temperature, thus enabling unprecedented control of exciton dynamics in 2D-TMDs. In addition, charge and energy transfer can be tuned on ultrafast time scales by tailoring the band alignment in vertically stacked hetero-bilayers and multilayers. While work on stacked monolayers of different kinds has been so far limited to bilayers, richer possibilities are offered by multilayers to control ultrafast energy, charge transfer, and excited state dynamics. Most of this territory is yet to be explored in 2D semiconductors.

7 Charge Transport

Besides light-induced excited state dynamics, steady-state carrier dynamics of relevance in electronics has been a main driver of recent investigations on 2D semiconductors, as briefly reviewed in this section. Advances in digital electronics have been driven by scaling down silicon transistors to improve performance, at a pace following so far the trends predicted by Moore's law [103]. The awareness that quantum effects inherently limit the possibility to scale transistors to the ~1 nm length scale using conventional approaches has motivated a search for nanomaterials and architectures to be employed in next-generation transistors and electronic circuits. In this context, the ideal nanomaterial would be able to combine good performance with low-cost, easy processing, and flexibility.

The very high carrier mobility of graphene (over $200,000 \text{ cm}^2/\text{Vs}$) [6, 7] has attracted applications in electronics, but the lack of a band gap limits the potential of graphene in its pure form for use in field effect transistors and optoelectronics [23]. Strategies to open a band gap in graphene – including chemical doping, nanostructuring into ribbons, or applying an electric field – typically deteriorate carrier mobility due to edge and impurities scattering. Semiconducting 2D materials such as 2D-TMDs conveniently combine subnanometer thickness, a band gap of 1–2 eV in the visible frequency range, and relatively high carrier mobility (e.g., up to $\sim 200 \text{ cm}^2/\text{Vs}$ in monolayer MoS_2) [14]. These materials are highly promising to support high on/off ratios in logic circuits with low power dissipation, while maintaining high carrier mobilities even at atomic-scale dimensions and room temperature [104]. An important breakthrough in the use of 2D-TMDs for nanoelectronics devices has been shown in work by Radisavljevic et al. [14], who realized the first field effect transistor with monolayer MoS_2 as the conductive channel and HfO_2 as the gate insulator with on/off current ratios of $\sim 10^8$ and mobilities of up to $200 \text{ cm}^2/\text{Vs}$ comparable to silicon technology. The same group also showed signal amplification and logic operations in simple integrated circuits using monolayer MoS_2 deposited on doped silicon [105].

A fundamental step to achieve high carrier mobility is the use of a high- κ gate dielectric. This result has been explained in terms of a reduced Coulomb scattering and a possible modification of phonon dispersion due to the dielectric material [14]. Further experimental evidence suggests that the dominant scattering mechanism at low temperature up to 200 K is the Coulomb scattering caused by charged impurities located within the monolayer, while at temperatures above 200 K, electron–phonon becomes the dominant scattering mechanism [104]. Recent computational work has estimated an upper limit for the mobility of defect-free n -type monolayer MoS_2 of $410 \text{ cm}^2/\text{Vs}$ at room temperature due to scattering with optical phonons [106]. We suggest that more work is necessary to understand scattering and mobility limits in 2D-TMDs.

Both n -type and p -type conduction has been reported in transistors based on intrinsic monolayer MoS_2 . The ambipolar behavior has been explained as the effect of defect traps and impurities at the interface with the gate dielectric [107]. This result can be understood by the fact that monolayer materials are thinner than the Debye screening length and are thus affected by impurities in the proximity of the material. For this reason, doping of 2D semiconductors by chemisorption of dopants on the substrate could be a viable strategy to engineer the electronic properties by

manipulating those of the substrate without altering the structure of the 2D material.

8 Emerging 2D materials

Novel materials beyond those discussed here are gaining attention in recent research. Some of these are worthy of mention as their study may guide future developments in the field. In particular, silicene – the silicon-based counterpart of graphene – is a semimetallic system consisting of a buckled 2D layer of Si atoms arranged in a honeycomb lattice [108]. Silicene has been grown epitaxially on Ag surfaces with different orientations. Angle resolved photoemission experiments and DFT calculations showed a band structure with Dirac cones analogous to graphene [109, 110]. Given the tendency of silicon to form sp^3 rather than sp^2 bonds, silicene sheets and nanoribbons are stable only if a small buckling of $\sim 0.4 \text{ \AA}$ is present. Unlike silicon surfaces, which are highly reactive to oxygen, silicene was found to be resistant to oxygen reactivity. While the computed mobility of silicene is close to that of graphene, growth of usable silicene layers is currently the main limiting factor. Though the growth of silicene has so far been limited to metallic substrates, several groups are working on growing silicene on insulators, which would allow for better investigation of its electronic and optical properties [111].

A family of recently investigated 2D materials is a group of early transition metal carbides and carbonitrides called MXenes, which have been reviewed in Ref. [112]. MXene monolayers are produced by etching so-called MAX bulk compounds with composition $\text{M}_{n+1}\text{AX}_n$, where M is an early transition metal, A is a group 13 or 14 element, X is carbon and/or nitrogen, and $n = 1, 2, \text{ or } 3$. The MAX structure can be described as 2D layers of M_{n+1}X_n early transition metal carbides and/or nitrides (e.g., Ti_2C or Ti_3CN) held together by chemical bonding with an A element. The strong M–X bond has a mixed covalent/ionic character, whereas the M–A bond is metallic. In contrast to other layered materials such as graphite and TMDs where weak van der Waals interactions hold the layers together, the bonds between the layers in the MAX phases are too strong to be broken by exfoliation. By taking advantage of the differences in bond strength, the A layers can be selectively etched by chemical means without disrupting the M–X bonds, thus allowing preparation of 2D MXenes [112]. Interestingly, this strategy to make 2D materials may be extended to other known families of bulk compounds. To date, the family of synthesized MXene ma-

materials includes Ti_3C_2 , Ti_2C , Nb_2C , V_2C , $(\text{Ti}_{0.5}, \text{Nb}_{0.5})_2\text{C}$, $(\text{V}_{0.5}, \text{Cr}_{0.5})_3\text{C}_2$, Ti_3CN , and Ta_4C_3 , though many more have been predicted theoretically [112]. The MXene monolayers consist of three, five, or seven atomic layers for M_2X , M_3X_2 and M_4X_3 , respectively, in all cases with a thickness of less than 1 nm. Most MXenes are metals with high conductivities comparable to multilayer graphene [113]. MXenes combine the metallic conductivity of transition metal carbides with the hydrophilic nature of their hydroxyl- or oxygen-terminated surfaces, and as such they behave as conductive clays [112], showing promise in applications for Li ion intercalation, catalysis, and electronics.

One last family of 2D materials of recent interest is derived from bulk methylammonium PbI perovskite, a material with a 1.6 eV gap that has recently found use in efficient solar cells [114]. In this mixed organic-inorganic halide perovskite, the methylammonium ions balance the charge of corner-sharing $[\text{PbI}_6]^{4-}$ octahedra [114]. By using longer hydrocarbon cations to increase the spacing of the PbI octahedra, layered 2D PbI perovskites with one, two, and three unit cell thickness have been recently synthesized. The monolayer and bilayer materials luminesce strongly and show a higher gap than the bulk value, which is restored for a thickness of roughly 3–4 layers [115]. In going from bulk to the 2D monolayer, the optical absorption gap increases by about 1 eV, and the exciton binding energy increases from 37 meV in bulk to 320 meV in 2D [115]. This near 10-fold increase reflects the weaker screening, similar to the case of 2D-TMDs. While research is still in the very early stage for these 2D semiconductors, their relevance in solar cell applications suggests that extensive studies will be carried out.

9 Applications

Modern electronic and optoelectronic devices typically require growth and/or controlled doping of semiconducting thin film materials. Advances in molecular beam epitaxy, CVD, and lithography have dramatically increased the capability to manufacture nanoscale devices using top-down processing of conventional semiconductors. Epitaxial growth of thin films of semiconductors and insulators has also achieved a high level of sophistication. However, the need to match the lattice parameters and structures of the substrate and deposited film severely limits the range of compatible materials, and interface defects and disorder are typically introduced during epitaxial growth. Given that the van der Waals interaction between 2D monolayers is free of epitaxial requirements, 2D materials with any

structure and composition can be stacked with arbitrary order and orientation, thus providing a paradigm shift in the manufacturing of novel heterojunctions. Put loosely, stacking 2D materials with van der Waals interactions is more like assembling Lego's than gluing layers together as in the case of stacking bulk crystalline materials. Although more work is necessary to achieve better control of CVD growth and transfer processes to create heterojunctions, progress so far has been rapid and encouraging, and the design of a new range of 2D heterostructures is within reach.

Applications in novel electronic, optoelectronic, and renewable energy devices abound for 2D semiconductors, both in the monolayer and multilayer forms. The extraordinary light absorption in 2D-TMDs, together with the possibility to dissociate excitons and separate charges at type-II interfaces, show promise for applications in photovoltaic (PV) solar cells. In addition, since the edges of TMD flakes can reduce water to hydrogen, application in photocatalytic cells have also been envisioned [116, 117]. Recently, we showed [37] that the three TMD monolayers MoS_2 , MoSe_2 , and WS_2 can absorb up to 5–10% incident sunlight in a thickness of less than 1 nm, thus achieving one order of magnitude higher sunlight absorption than commonly employed PV materials such as GaAs and Si. We further studied PV devices based on just two stacked monolayers: (1) a Schottky barrier solar cell between MoS_2 and graphene, and (2) an excitonic solar cell based on a type-II MoS_2/WS_2 hetero-bilayer [37]. We demonstrated that such 1 nm thick active layers can attain power conversion efficiencies of up to ~1%, corresponding to 100–1,000 times higher power densities (Watts/kg) than the best existing ultrathin solar cells [37]. The predicted type-II alignment and charge separation for the MoS_2/WS_2 hetero-bilayer have both been observed in recent experiments [46, 71], and a MoS_2/WS_2 solar cell with close to 1% efficiency has been experimentally shown recently [118].

While the predicted 1% power conversion efficiency is one order of magnitude too low for PV applications, the efficiency could be increased using a number of strategies in a real device. For example, since the absorbance of graphene and MoS_2 has been shown to double and triple, respectively, for a bilayer and trilayer, a stacking of three graphene monolayers and three MoS_2 monolayers with a back metallic contact to double the light path could afford maximum efficiencies close to 10% in a ~3 nm thick active layer [37]. Significant band gap engineering is possible using stacked TMD hetero-bilayers and multi-layers. For example, TMD heterostructures may enable fabrication of multijunction solar cells free of epitaxial strain, in which light absorption and exciton dynamics are con-

trolled within each stacked monolayer. In summary, we believe 2D monolayer materials hold yet untapped potential for solar energy absorption and conversion at the nanoscale.

The ability to control exciton dynamics in 2D-TMDs has great relevance in optoelectronic applications. Tunable PL frequency and radiative lifetimes hold unique potential for the development of novel light emitting diodes (LEDs) and lasers based on TMDs. While the role of defects in light emission is still poorly understood in these materials, the approaches described above to increase brightness are encouraging toward the realization of a new family of ultrathin LEDs based on 2D-TMDs.

Given their flat nature, 2D materials show unique potential to fabricate flexible and ultrathin devices. Different from other PV materials amenable to thin film fabrication on flexible substrates, such as conjugated polymers and small molecules, 2D-TMDs show carrier mobilities similar to bulk semiconductors, and are also stable when exposed to air and moisture. Experience shows that optical absorption and mobility of 2D-TMDs left in ambient condition do not change significantly over time. On the other hand, some groups reported that the PL appears to degrade after weeks of storage in the lab in ambient conditions – for reasons yet to be clarified – so that storage under low vacuum is common when handling 2D-TMDs for light emission. More studies are necessary on the stability of 2D-TMDs under air and light exposure to establish whether encapsulation is needed in real devices. The trajectory so far suggests that the next decade of work on 2D materials will bring them one step closer to real-world applications.

10 Conclusions

This review article emphasized several aspects of the electronic and optical properties of 2D semiconductors, and how these differ from the properties of bulk materials. Fabrication of ultrathin and flexible devices is the ultimate goal of applied research on 2D materials, while the strong light–matter interaction is a fundamental aspect still under intense investigation. The weak screening, strong light–matter interaction, and strongly bound excitons are inherent to the low-dimensional nature of 2D materials. The strong impact of defects on the optical and electronic properties is also general, and may also be seen as a consequence of weak screening. The remarkable tunability of the optical properties in 2D-TMDs and the possibility to modulate carrier mobility by changing the sur-

face chemistry of the substrate are novel aspects of great practical interest. The weak screening and the sensitivity of 2D semiconductors to the external environment and to internal perturbation from defects suggests that 2D materials should be seen as “naked” systems exposing their electronic states to the environment. It is our challenge to take advantage of these naked electrons to improve current technology.

Acknowledgement: M.B. acknowledges support by a start-up fund from the California Institute of Technology. M.P. acknowledges E.C. for the RISE Project CoExAN GA644076. J.C.G. and C.A. are grateful to the Eni Solar Frontiers Center for financial support.

References

- [1] B. G. Streetman, and S. Banerjee, *Solid State Electronic Devices*, 7th Ed. (Prentice-Hall Englewood Cliffs, NJ, 1995).
- [2] J. Wilson, and J. F. Hawkes, *Optoelectronics – An Introduction*, 2nd Ed. (Prentice Hall, Englewood Cliffs, NJ, 1989).
- [3] A. Cho, and J. Arthur, *Prog. Solid State Chem.* 1975, 10, 157–191.
- [4] A. K. Geim, and K. S. Novoselov, *Nature Mater.* 2007, 6, 183–191.
- [5] K. S. Novoselov, et al., *Science* 2004, 306, 666–669.
- [6] A. K. Geim, *Science* 2009, 324, 1530–1534.
- [7] A. H. Castro Neto, F. Guinea, N. M. R. Peres, K. S. Novoselov, and A. K. Geim, *Rev. Mod. Phys.* 2009, 81, 109–162.
- [8] A. Splendiani, et al., *Nano Lett.* 2010, 10, 1271–1275.
- [9] K. S. Novoselov, et al., *Proc. Natl. Acad. Sci. USA* 2005, 102, 10451–10453.
- [10] X. Li, et al., *Science* 2009, 324, 1312–1314.
- [11] K. K. Kim, et al., *Nano Lett.* 2012, 12, 161–166.
- [12] Y.-H. Lee, et al., *Adv. Mater.* 2012, 24, 2320–2325.
- [13] K. F. Mak, C. Lee, J. Hone, J. Shan, and T. F. Heinz, *Phys. Rev. Lett.* 2010, 105, 136805.
- [14] B. Radisavljevic, A. Radenovic, J. Brivio, V. Giacometti, and A. Kis, *Nature Nanotech.* 2011, 6, 147–150.
- [15] H. Wang, et al., *Nano Lett.* 2012, 81, 109–162.
- [16] R. S. Sundaram, et al., *Nano Lett.* 2013, 13, 1416–1421.
- [17] F. Bassani, and G. P. Parravicini, *Electronic States and Optical Transitions in Solids*, Pergamon, 1975.
- [18] G. Onida, L. Reining, and A. Rubio, *Rev. Mod. Phys.* 2002, 74, 601–659.
- [19] M. S. Hybertsen, and S. G. Louie, *Phys. Rev. B* 1986, 34, 5390–5413.
- [20] T. Ohta, A. Bostwick, T. Seyller, K. Horn, and E. Rotenberg, *Science* 2006, 313, 951–954.
- [21] Y. Zhang, et al., *Nature* 2009, 459, 820–823.
- [22] K. S. Novoselov, *Rev. Mod. Phys.* 2011, 83, 837–849.
- [23] P. Avouris, and C. Dimitrakopoulos, *Mater. Today* 2012, 15, 86–97.
- [24] P. Avouris, *Nano Lett.* 2010, 10, 4285–4294.
- [25] M. Chhowalla, et al., *Nature Chem.* 2013, 5, 263–275.
- [26] C. Ataca, H. Sahin, and S. J. Ciraci, *Phys. Chem. C* 2012, 116, 8983.

- [27] T. Cheiwchanamngij, and W. R. L. Lambrecht, *Phys. Rev. B* 2012, 85, 205302.
- [28] Y. Zhang, et al., *Nature Nanotech.* 2014, 9, 111–115.
- [29] W. Zhao, et al., *ACS Nano* 2013, 7, 791–797.
- [30] H. R. Gutierrez, et al., *Nano Lett.* 2013, 13, 3347–3454.
- [31] Z. Zhu, Y. Cheng, and U. Schwingenschlöggl, *Phys. Rev. B* 2011, 84, 153402.
- [32] D. Xiao, G.-B. Liu, W. Fenf, X. Xu, and W. Yao, *Phys. Rev. Lett.* 2012, 108, 196802.
- [33] P. Cox, *Transition Metal Oxides*, Clarendon Press, Oxford, 1992.
- [34] R. M. Martin, *Electronic Structure: Basic Theory and Practical Methods*, Cambridge University Press, 2008.
- [35] D. Qiu, F. H. Da Jornada, and S. G. Louie, *Phys. Rev. Lett.* 2013, 111, 216805.
- [36] J. K. Ellis, M. J. Lucero, and G. E. Scuseria, *Appl. Phys. Lett.* 2011, 99, 261908.
- [37] M. Bernardi, M. Palummo, and J. C. Grossman, *Nano Lett.* 2013, 13, 3664–3670.
- [38] S. Tongay, et al., *Nano Lett.* 2012, 12, 5576–5580.
- [39] S. Tongay, et al., *Sci. Rep.* 2013, 3, 2657.
- [40] S. Tongay, et al., *Nano Lett.* 2013, 13, 2831–2836.
- [41] F. Capasso, and G. Margaritondo, *Heterojunction Band Discontinuities: Physics and Device Applications*, North Holland, 1987.
- [42] K. Kosmider, and J. Fernandez-Rossier, *Phys. Rev. B* 2013, 87, 075451.
- [43] J. Kang, S. Tongay, J. Zhou, J. Li, and J. Wu, *Appl. Phys. Lett.* 2013, 102, 012111.
- [44] Y. Liang, S. Huang, R. Soklaski, and L. Yang, *ArXiv e-prints:1306.0620v2*, 2014.
- [45] M. Bernardi, M. Palummo, and J. C. Grossman, *ACS Nano* 2012, 6, 10082–10089.
- [46] X. Hong, et al., *Nature Nanotech.* 2014, 9, 682–686.
- [47] W. J. Zhang, et al., *Sci. Rep.* 2014, 4, 3826.
- [48] R. Shaltaf, G.-M. Rignanese, X. Gonze, F. Giustino, and A. Pasquarello, *Phys. Rev. Lett.* 2008, 100, 186401.
- [49] N. W. Ashcroft, and N. D. Mermin, *Solid State Physics*, Saunders, Philadelphia, 1976.
- [50] F. Huser, T. Olsen, and K. Thygesen, *Phys. Rev. B* 2013, 88, 245309.
- [51] A. Ramasubramaniam, *Phys. Rev. B* 2012, 86, 115409.
- [52] M. M. Ugueda, et al., *Nature Mater.* 2014, DOI:10.1038/nmat4061
- [53] W. L. Barnes, A. Dereux, and T. W. Ebbesen, *Nature* 2003, 424, 824–830.
- [54] M. Jablan, M. Soljacic, and H. Buljan, *Proc. IEEE* 2013, 101, 1689–1704.
- [55] Y. Liu, R. F. Willis, K. V. Emtsev, and T. Seyller, *Phys. Rev. B* 2008, 78, 201403.
- [56] R. R. Nair, et al., *Science* 2008, 320, 1308.
- [57] L. Yang, J. Deslippe, C.-H. Park, M. L. Cohen, S. G. Louie, *Phys. Rev. Lett.* 2009, 103, 186802.
- [58] L. Britnell, et al., *Science* 2013, 340, 1311–1314.
- [59] D. Kozawa, et al., *Nature Commun.* 2014, 5, 4543.
- [60] W. Zhao, et al., *ACS Nano* 2013, 7, 791–797.
- [61] Z. Ye, et al., *Nature* 2014, 513, 214–218.
- [62] M. Palummo, M. Bernardi, J. C. Grossman, *Nano Lett.* 2015, 15, 2794–2800
- [63] K.F. Mak, et al., *Nature Mater.* 2013, 12, 207–211.
- [64] J. S. Ross, *Nature Commun.* 2013, 4, 1474.
- [65] S. Mouri, Y. Miyauchi, and K. Matsuda, *Nano Lett.* 2013, 13, 5944–5948.
- [66] J. Feng, X. Qian, C.-W. Huang, and J. Li, *Nature Photon.* 2012, 6, 866–872.
- [67] A. P. Nayak, et al., *Nature Commun.* 2014, 5, 3731.
- [68] R. Soklaski, Y. Liang, and L. Yang, *Appl. Phys. Lett.* 2014, 104, 193110.
- [69] A. Molina-Sanchez, D. Sangalli, K. Hummer, A. Marini, and L. Wirtz, *Phys. Rev. B* 2013, 88, 045412.
- [70] H. Terrones, F. Lopez-Urias, and M. Terrones, *Sci. Rep.* 2013, 3, 1549.
- [71] P. Rivera, et al., *ArXiv e-prints*, 1403.4985, 2014.
- [72] Y. Yu, et al., *ArXiv e-prints*, 1403.6181, 2014.
- [73] H.-P. Komsa, and A. V. Krasheninnikov, *Phys. Rev. B* 2013, 88, 085318.
- [74] A. A. Bakulin, et al., *Science* 2012, 335, 1340–1344.
- [75] A. A. High, E. E. Novitskaya, L. V. Butov, M. Hanson, and A. C. Gossard, *Science* 2008, 321, 229–231.
- [76] T. Cao, et al., *Nature Commun.* 2012, 3, 887.
- [77] K. F. Mak, K. L. He, J. Shan, and T. F. Heinz, *Nature Nanotech.* 2012, 7, 494–498.
- [78] H. L. Zeng, et al., *Nature Nanotech.* 2012, 7, 490–493.
- [79] A. M. Jones, et al. *Nature Nanotech.* 2013, 8, 634–638.
- [80] N. M. Gabor, et al., *Science* 2011, 334, 648–652.
- [81] J. C. W. Song, M. S. Rudner, C. M. Marcus, and L. S. Levitov, *Nano Lett.* 2011, 11, 4688–4692.
- [82] M. Freitag, T. Low, F. Xia, and P. Avouris, *Nature Photon.* 2013, 7, 53–59.
- [83] R. Bistritzer, and A. H. MacDonald, *Phys. Rev. Lett.* 2009, 102, 206410.
- [84] M. W. Graham, S.-F. Shi, D. C. Ralph, J. Park, and P. L. McEuen, *Nature Phys.* 2013, 9, 103–108.
- [85] L. Ju, et al., *Nature Nanotech.* 2011, 6, 630–634.
- [86] A. N. Grigorenko, M. Polini, and K. S. Novoselov, *Nature Photon.* 2012, 6, 749–758.
- [87] A. Scholz, T. Stauber, and J. Schliemann, *Phys. Rev. B* 2013, 88, 035135.
- [88] F. Bonaccorso, Z. Sun, T. Hasan, and A. C. Ferrari, *Nature Photon.* 2010, 4, 611–622.
- [89] X. Wei, et al., *AIP Adv.* 2014, 4, 123004.
- [90] G. Eda, S. A. Maier, *ACS Nano* 2013, 7, 5660–5665.
- [91] J. Heber, *Nature Phys.* 2014, DOI:10.1038/nphys3147
- [92] T. Korn, S. Heydrich, M. Hirmer, J. Schmutzler, and C. Schüller, *Appl. Phys. Lett.* 2011, 99, 102109.
- [93] D. Lagarde, et al., *Phys. Rev. Lett.* 2014, 112, 047401.
- [94] H. Shi, et al., *ACS Nano* 2013, 7, 1072–1080.
- [95] N. Peimyoo, et al., *ACS Nano* 2013, 7, 10985–10994.
- [96] G. Grancini, et al., *Nature Mater.* 2013, 12, 29–33.
- [97] S. Gelinas, et al., *Science* 2013, 343, 512–516.
- [98] A. E. Jilaubekov, et al., *Nature Mater.* 2013, 12, 66–73.
- [99] M. Bernardi, D. Vigil-Fowler, J. Lischner, J. B. Neaton, and S. G. Louie, *Phys. Rev. Lett.* 2014, 112, 257402.
- [100] C. A. Rozzi, et al., *Nature Commun.* 2013, 4, 1602.
- [101] S. Falke, et al., *Science* 2014, 344, 1001–1005.
- [102] D. Sangalli, and A. Marini, *ArXiv e-prints*, 1409.1706, 2014.
- [103] S. E. Thompson, and S. Parthasarathy, *Mater. Today* 2006, 9, 20–25.
- [104] B. Radisavljevic, and A. Kis, *Nature Mater.* 2013, 12, 815–820.
- [105] B. Radisavljevic, M. B. Whitwick, and A. Kis, *ACS Nano* 2011, 5, 9934–9938.

- [106] K. Kaasbjerg, K. S. Thygesen, and K. W. Jacobsen, *Phys. Rev. B* 2012, 85, 115317.
- [107] K. Dolui, I. Rungger, and S. Sanvito, *Phys. Rev. B* 2013, 87, 165402.
- [108] B. Lalmi, et al., *Appl. Phys. Lett.* 2010, 97, 223109.
- [109] P. Vogt, et al., *Phys. Rev. Lett.* 2012, 108, 155501.
- [110] A. Kara, et al., *Surf. Sci. Rep.* 2012, 67, 1–18.
- [111] S. Orres, *Proc. Natl. Acad. Sci. USA* 2014, 111, 10899.
- [112] M. Naguib, V. N. Mochalin, M. W. Barsoum, and Y. Gogotsi, *Adv. Mater.* 2014, 26, 992–1005.
- [113] M. Naguib, et al., *ACS Nano* 2012, 6, 1322–1331.
- [114] S. Stranks, et al., *Science* 2013, 342, 341–344.
- [115] L. Brus, *Acc. Chem. Res.* 1014, DOI: 10.1021/ar500175h
- [116] T. F. Jaramillo, et al., *Science* 2007, 317, 100–102.
- [117] J. Kibsgaard, Z. Chen, B. N. Reinecke, and T. F. Jaramillo, *Nature Mater.* 2012, 11, 963–969.
- [118] M. M. Furchi, et al., *Nano Lett.* 2014, 14, 4785–4791